Journal of Alloys and Compounds 525 (2012) 1–7

Contents lists available at SciVerse ScienceDirect

Journal of Alloys and Compounds

journal homepage: www.elsevier.com/locate/jallcom

Morphology evolution of ZnO thin films from aqueous solutions and their application to liquefied petroleum gas (LPG) sensor

K.V. Gurav[a,b], U.M. Patil[a], S.W. Shin[b], S.M. Pawar[b], J.H. Kim[b,*], C.D. Lokhande[a,*]

[a] Thin Film Physics Laboratory, Department of Physics, Shivaji University, Kolhapur 416 004, M.S. India
[b] Photonic and Electronic Thin Film Laboratory, Department of Materials Science and Engineering, Chonnam National University, Gwangju 500-757, South Korea

ARTICLE INFO

Article history:
Received 10 November 2010
Received in revised form 11 January 2012
Accepted 16 January 2012
Available online xxx

Keywords:
Chemical deposition
Vertically aligned ZnO rods
ZnO flakes
XRD
SEM
LPG sensor

ABSTRACT

The chemical bath deposition method is used to prepare two-dimensional flakes and one-dimensional rods of ZnO. By changing the bath temperature, ZnO morphology can be changed from flakes to rods. Further orientation of ZnO rods are selectively controlled by varying the content of H_2O_2 in the bath solution. These films are structurally and morphologically characterized using X-ray diffraction and scanning electron microscopy respectively. The dependence of liquefied petroleum gas (LPG) sensing properties on morphology and orientation of ZnO thin film are investigated. The vertically aligned ZnO rods exhibited the maximum gas response of 49% at 573 K upon exposure to 5200 ppm of LPG.

1. Introduction

Zinc oxide (ZnO) has played an inevitable role among all the other metal oxides for many applications, due to its unique combination of interesting properties, such as non-toxicity, good electrical conductivity and lower cost [1]. ZnO is a promising candidate for optoelectronics and piezoelectric applications due to its wide band gap (3.37 eV), a large exciton binding energy (60 meV) at room temperature and its non-centro-symmetry in the wurtzite structure [2]. ZnO can be grown richest variety of nanostructures [3] and is expected to be the next most important material for a variety of practical applications such as TCOs [4], photodetectors [5], UV-laser [6], gas sensors [7,8], buffer layers in CIS solar cells [9], n-type window layer in extremely thin absorber (ETA) solar cells [10], and as an electrode in DSSCs [11,12]. Until today, there has been a prevailing need for efficient, low temperature and low-cost deposition methods for thin films as technological industrial applications. Over the past few years, many methods such as magnetron sputtering [13], chemical vapour deposition [14], pulsed laser deposition [6], spray pyrolysis [15], sol–gel [5], electrodeposition [11] and hydrothermal [16] have been employed to synthesize nanostructured ZnO thin films.

Chemical bath deposition (CBD) is a soft chemical method used to deposit thin films from aqueous solution, with advantages such as low processing temperature, allowing growth on a variety of substrates, and easy adaptation to large area processing with low fabrication cost [17]. Thus this method has been preferred option over the expensive methods. In order to improve physical and chemical performance of devices, engineering of ZnO morphology is focus of current research. Control of crystal growth for this purpose can be conducted by CBD, in which small degree of supersaturation of the solutions causes the heterogeneous nucleation of the metal oxide on the substrates [18]. Many studies have reported on the synthesis of various ZnO morphologies by chemical method [19–25].

Ma et al. [19] have prepared three-dimensional porous ZnO structure by chemical method. They have shown ZnO morphology evolves from ZnO spheres, lamellar to stacked nanoplates by varying concentration of trisodium citrate in the bath solution and that can be used for photocatalysis. Kulkarni et al. have shown the temperature impact on morphological evolution of ZnO and its consequent effect on the physio-chemical properties [20]. Xu et al. [21] have successfully realized preliminary control over assembly pattern of ZnO architectures (rod like, flowerlike, urchin like, stelliform, and rod arrays) by varying different substrates including glass, Pt/glass, Au/glass, and ITO/glass through a CBD method. Further, they have proposed possible growth mechanisms for different assembly patterns on the substrates. Urgessa et al. [22] have been reported the effect of VI/II ratio on the growth of ZnO structures using a simple chemical bath deposition method. They have

* Corresponding authors.
E-mail addresses: gkishor7283@yahoo.com (K.V. Gurav), jinhyeok@chonnam.ac.kr (J.H. Kim), l_chandrakant@yahoo.com (C.D. Lokhande).

0925-8388/$ – see front matter © 2012 Elsevier B.V. All rights reserved.
doi:10.1016/j.jallcom.2012.01.082

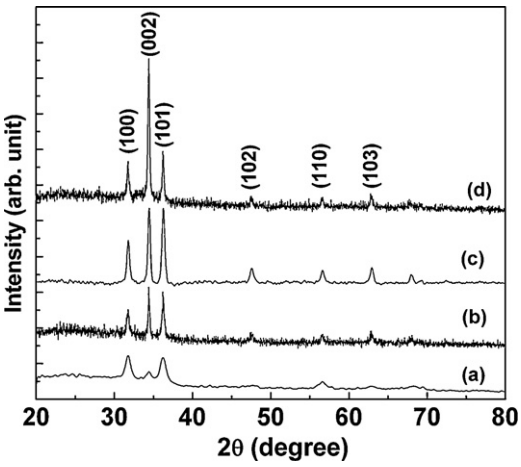

Fig. 1. The XRD patterns of ZnO thin films deposited for samples (a) Z1 (303 K) (b) Z2 (333 K) (c) Z3 (348 K) and (d) Z4 (363 K).

shown transition from quasi-spherical particles to rods as the VI/II ratio is varied from 1 to 40 ZnO morphological transformation from rod-to-disk to spindle-to-flower by varying pH of the bath solution have been observed by Pawar et al. [23]. Further they have studied PEC properties of various ZnO structures. Duan et al. [24] reported the morphology-controlled synthesis of ZnO films with gelatin via CBD. Different ZnO microstructures ranging from hexagonal prisms, plates to rose-like twinned crystals are prepared through varying the concentration of gelatin. A recent study by Yuan et al. shows that, size of ZnO nanoarray scan be well tuned by varying the concentration of the precursor and stirring time [25].

Recently, liquefied petroleum gas (LPG) sensing properties of various ZnO microstructures such as flakes [26], flowers [27], rods [28,29], leafs [30], needles [31], have been reported. However the effect of ZnO morphology on LPG sensing properties has been scarcely reported [32]. Recently, improved sensing performance for vertically aligned ZnO rods than that of entangled ones has been reported [33].

In this paper, we report on chemical synthesis of ZnO thin films. The effect of bath temperature on the morphology evolution is investigated. In addition the effect of morphology and rod orientation on LPG sensing properties is also evaluated and reported.

2. Experimental details

2.1. Synthesis of ZnO microstructures

In typical synthesis of ZnO microstructures, an aqueous NH_3 solution (28%) was added into freshly prepared 0.1 M $Zn(NO_3)_2$ solution under constant stirring condition. Initially, white precipitate of $Zn(OH)_2$ was observed, further addition of the NH_3 resulted to form a clear zincate solution by dissolving the precipitate. The pH of resultant solution was ~12. The solution was stirred for few seconds and then transferred into another beaker containing ultrasonically cleaned glass substrates inclined vertically at 20° to the walls of the beaker. The bath solution maintained at different bath temperatures (room temperature (303 K), 333, 348 and 363 K) were utilized for the deposition. After a predetermined time interval, at different bath temperatures (303–363 K) the substrates coated with ZnO were removed, washed with double distilled water dried in air and preserved in the vacuum desiccator. The deposited films were air annealed at 673 K for 2 h. The ZnO thin films deposited with bath temperature 303, 333, 348 and 363 K, and annealed at 673 K for 2 h are hereafter denoted as samples Z1, Z2, Z3 and Z4, respectively.

2.2. Synthesis of ZnO rods

The clear zincate solution with pH ~12 was prepared from the aqueous alkaline solution of $Zn(NO_3)_2$ as discussed in the preceding section. The hydrogen peroxide (H_2O_2 30 vol.%) was added into the solution with different volumetric proportions results into decrease in pH of the solution. The pH of the solution was maintained at ~12 by addition of NH_3 solution. The pre-cleaned glass substrates were immersed and placed vertically in the solution. The solution was maintained at bath temperature 348 K for 2 h, resulting in the direct growth of ZnO rods onto the glass substrate. The substrates with ZnO deposit were thoroughly washed with deionized water to remove residual salts, and dried at similar temperature. The ZnO thin films deposited from the solution bath containing 0, 1 and 2 vol.% of H_2O_2 were annealed at 673 K for 2 h and hereafter referred as samples Z3, Z31 and Z32, respectively.

2.3. Characterization technique

The phase identification of the sample deposited on the glass substrate was investigated by using, X-ray diffractometer (XRD) using Cu-Kα_1 radiation [λ = 1.5406 Å] in the 2θ range from 20° to 80° (Philips PW-1710). The morphology of the samples was observed by using scanning electron microscopy (SEM, Model JEOL -6330). To measure gas sensing properties, test sample was placed in a sealed chamber and resistivity of the sample was measured in air (i.e. R_a), then LPG was injected into the chamber and the resistivity of the sample in presence of LPG was measured (i.e. R_g). We defined gas response of our gas sensors as follows

$$S(\%) = \left[\frac{(R_a - R_g)}{R_a}\right] \times 100 \quad (1)$$

3. Results and discussion

3.1. 3.1 Effect of bath temperature

Fig. 1(a)–(d) shows the XRD patterns of annealed ZnO thin films deposited at different bath temperatures. From figure it is observed that, all the samples show a polycrystalline nature. The peaks can be assigned to the (1 0 0), (0 0 2), (1 0 1), (1 0 2), (1 1 0) and (1 0 3) planes of a hexagonal wurtzite crystal structure of ZnO (JCPDS 36-1451). The crystal planes become more prominent with increasing bath temperature, which means crystallinity of the films is improved.

The effect of bath temperature on the microstructures of ZnO films annealed at 673 K was studied from SEM images. Fig. 2(a)–(d) shows SEM images of annealed ZnO samples deposited at different bath temperatures. Evolution in the ZnO film morphology with the bath temperature was observed. The interconnected flakes with porous surface are obtained for sample deposited at room temperature (sample Z1). The pores having diameter 1.5–2 μm are clearly seen between the interconnected ZnO flakes, the average thickness of the flakes are in the range of few tens of nanometers (Fig. 2(a)). With an increase in bath temperature above room temperature, the morphology evolves substantially and ZnO nanorods are formed as shown in Fig. 2(b) and (c). Sample Z2, prepared at bath temperature 333 K shows the formation of immature rods. When the bath temperature was increased from 333 to 348 K, the SEM image of the obtained sample Z3 (Fig. 2(c)) shows well-defined hexagonal facets ZnO rods of typical diameter 200 nm. Further increase in bath temperature to 353 K (sample Z4, Fig. 2(d)) resulted into the increase in rod diameter to 300 nm. The morphological evolution with increase in bath temperature may be due to the fact that bath temperature strongly affects the release of the Zn^{2+} ions from the zinc complex [$Zn(NH_3)_4^{2+}$]. At room temperature, slow release of Zn^{2+} ions leads to the formation of the flake-like morphology, while with increased bath temperature; the Zn^{2+} ions are released more quickly to form ZnO rods.

3.2. Effect of content of H_2O_2 in the bath solution

Fig. 3(a)–(c) shows the XRD patterns of the annealed ZnO films deposited at 348 K with different content of H_2O_2 in the bath solution. All the samples show the formation of ZnO with hexagonal wurtzite crystal structure (JCPDS 36-1451). It is interesting to note that, with increasing the content of H_2O_2, intensity of the (0 0 2) peak plane is markedly increased and that for other crystal planes disappeared or very weak, i.e. crystallites oriented strongly along *c*-axis. This may be due to the inhabitant ZnO crystal growth along *c*-axis, which is further promoted by adding H_2O_2 in the bath solution, which acts as the source of O^{2-} ions.

Fig. 4(a)–(f) shows SEM images of annealed ZnO thin films deposited with different contents of H_2O_2 in the bath solution at

two different magnifications (10 K and 50 K). Fairly, well defined hexagonal facets, entangled rods; typically having diameter of 200 nm is observed for sample Z3. Such rods are arranged in a very large, uniform array, which covers entire surface of the glass substrate, as shown in Fig. 4(a). Well defined crystallographic faces i.e. polar terminated (0 0 1) and non-polar (1 0 1) faces can clearly be identified [Fig. 4(b)]. Addition of H_2O_2 (1 vol.%) in bath solution (sample Z31) causes crystal to orient perpendicular to the substrate surface as shown in Fig. 4(c) and (d). With more H_2O_2 (2 vol.%) in the bath solution, vertically aligned ZnO rods are observed as shown in Fig. 4(e) and (f). This is attributed to the increased orientation of ZnO rods by increasing content of H_2O_2 in the bath solution. Fig. 4(g) shows the cross sectional view of the vertically aligned ZnO rods observed for sample Z32. It is seen that the ZnO crystals grow along *c*-axis and form vertically aligned ZnO rods.

3.3. Gas sensing properties

3.3.1. Gas sensing mechanism

The oxygen vacancy in ZnO thin film acts as an electron donor in ZnO and makes it as an n-type semiconductor [34]. The exposed surface of ZnO microstructure adsorbs the oxygen molecules from the ambient gas components, which capture conduction electrons and form O^-, given as [29].

$$O_{2(g)} + 2e^- \rightarrow 2O^-_{(ads)} \quad (2)$$

The ZnO microstructure provides high surface area results in high quantity of surface atoms, which can lead to the insufficiency of surface atomic coordination and high surface energy [35]. Therefore, the surface is highly active, which promotes further adsorption of oxygen in the ambient atmosphere. When the sensors are exposed to the reducing gases, for instance, LPG, the gas will react with the adsorbed O^-, as shown in Eq. (2) and released the trapped electrons back to the conduction band. This leads to an increased carrier concentration of ZnO and decreasing the resistance of the sensors [29].

$$C_nH_{2n+2} + 2O^- \rightarrow C_nH_{2n}\text{-}O + H_2O + e^- \quad (3)$$

where, C_nH_{2n+2}, represents the CH_4, C_3H_8 and C_4H_{10}.

3.3.2. Effect of morphology: bath temperature effect

Fig. 5 shows the gas response as a function of operating temperature for ZnO films obtained at different bath temperatures, under the exposure of 2600 ppm of LPG in air. From figure it is revealed that each sample exhibited maximum response at 673 K. In this case, at low operating temperatures, the sensor response is restricted by the speed of the chemical reaction, and at higher operating temperatures it is restricted by the speed of diffusion of gas molecules. At some intermediate temperature, the speed values of the two processes become equal, and at that point the sensor response reaches its maximum [28]. Thus, in the present case the optimum operating temperature for ZnO films is 673 K at which sensor response attained its peak value. The temperature, which corresponds to a certain peak value, is a function of the kind of target gases, the chemical composition of the oxide, including the additives and the catalysts, and the pure oxides are generally stable at lower temperatures. Hence, the high operating temperature is necessary for pure ZnO films to interact with the LPG [28].

Further, it is observed from Fig. 5 that at operating temperature 673 K, sample Z3 exhibited highest gas response (24%), compared to samples Z1 (14%), Z2 (18%) and Z4 (12%). This data shows LPG response is strongly depends on the ZnO morphology. It is well known that the gas response of the metal-oxide semiconductor sensors is mainly determined by the interactions between a target gas and the surface of the sensors. So, it is obvious that for the greater surface area of the materials, the interaction between the adsorbed gases and the sensor surface is stronger, i.e., the gas response is higher [32].

In the present case, it has been clearly seen from SEM images that for sample Z3, the well-defined hexagonally faceted rods

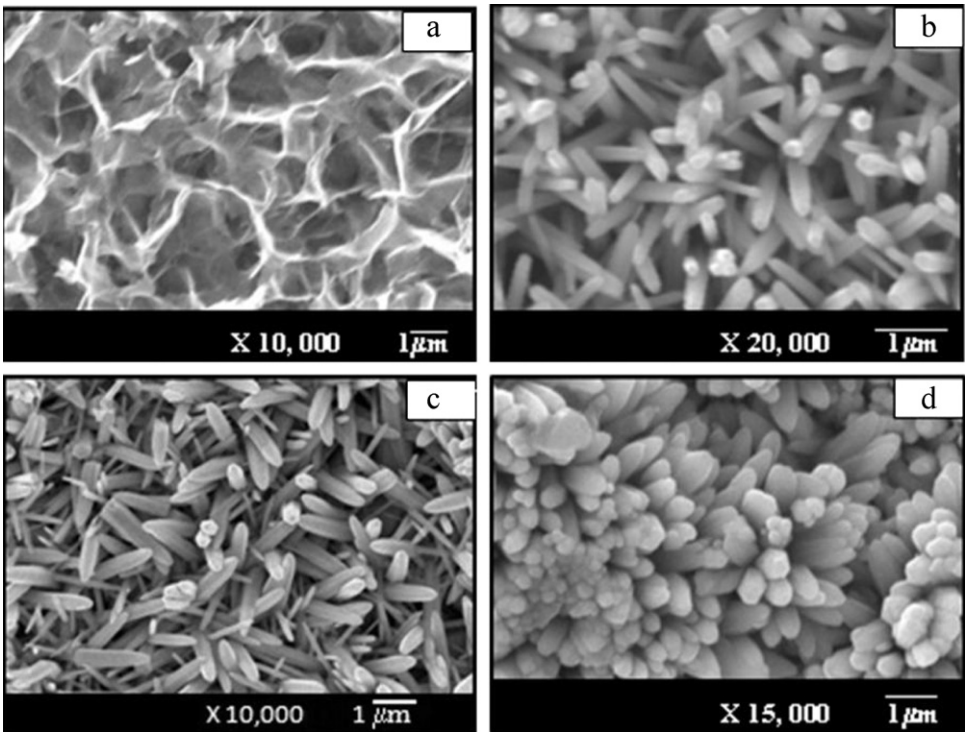

Fig. 2. Scanning electron micrographs for the samples (a) Z1 (303 K) (b) Z2 (333 K) (c) Z3 (348 K) and (d) Z4 (363 K).

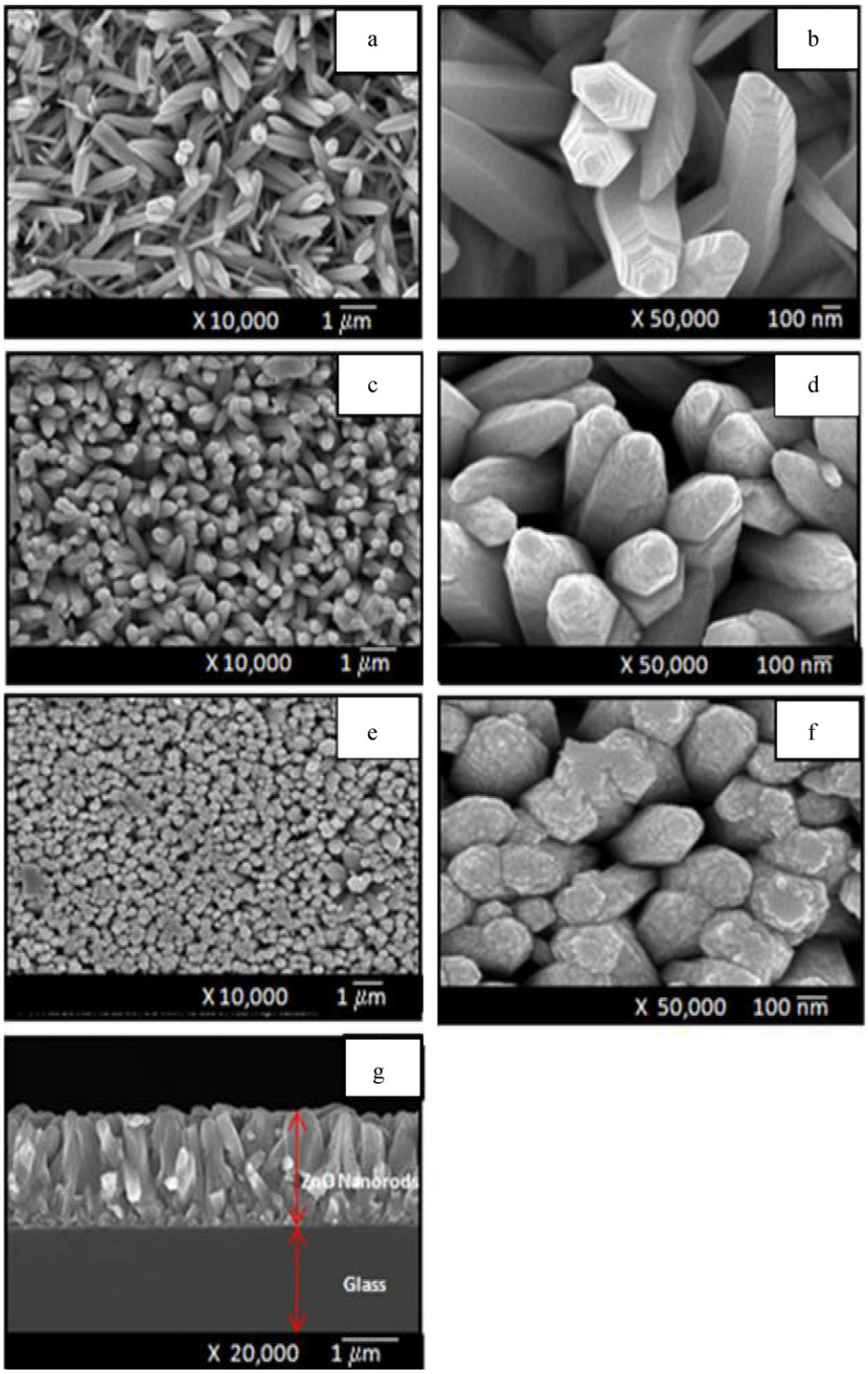

Fig. 4. (a)–(f) Scanning electron micrographs of sample Z3, Z31 and Z32 at two different magnifications (×10,000 and ×50,000) and (g) cross-sectional view of the sample Z32.

with average diameter of 200 nm offers more surface area to interact gas molecules, than that of interconnected flakes with microporous surface, immature rods and dense rods with average diameter 300 nm observed for sample Z1, Z2 and Z4, respectively. The surface area is largest for sample Z3, with largest number of adsorption–desorption sites, the response could be improved by the significant change in surface area. This is consistent with the expectation of the relatively higher response based on their larger surface-to-volume ratio. The sensor performance obtained in this work is definitely better than our earlier report [7], in which we have reported the maximum response of 12% to 2600 ppm of LPG by using fibrous ZnO flakes.

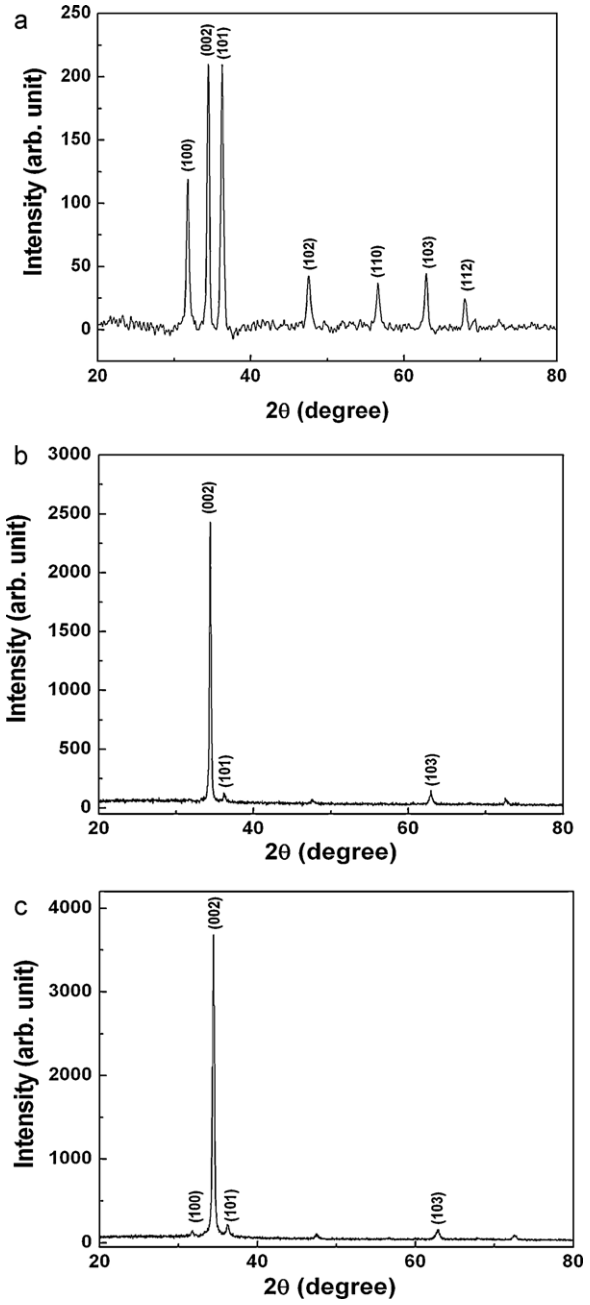

Fig. 3. X-ray diffractograms of sample (a) Z3 (without H_2O_2) (b) Z31 (with 1 vol.% H_2O_2) and (c) Z32 (with 2 vol.% H_2O_2).

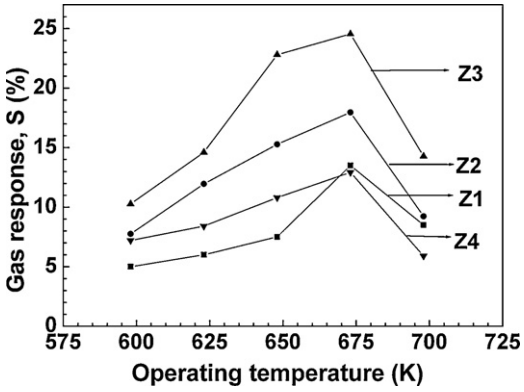

Fig. 5. LPG response as a function of operating temperature for ZnO films obtained at different bath temperatures (samples Z1–Z4) upon exposure to 2600 ppm of LPG.

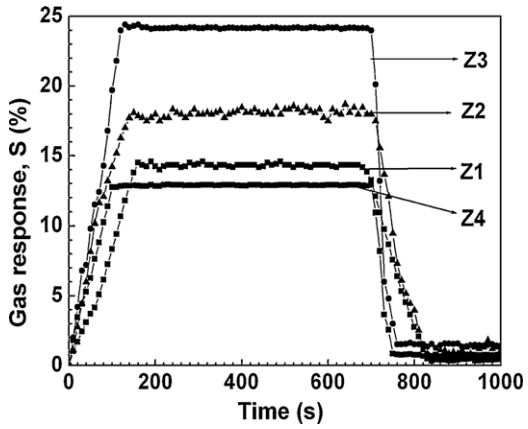

Fig. 6. Response transient curves of ZnO films obtained at different bath temperatures (samples Z1–Z4) upon exposure to 2600 ppm of LPG.

The transient curve for the samples Z1–Z4 upon exposure of 2600 ppm of LPG at 673 K is shown in Fig. 6. When the LPG was introduced in the gas chamber, the gas response initially increased with the operation time and then remained stable. The sample Z3 shows maximum response (24%). Fig. 7 shows the response and recovery times for samples Z1–Z4 operated at 673 K. The response time is defined as time require to reach 90% of saturation resistance upon exposure to test (LPG) gas and recovery time is defined as time required for recovering 90% of original resistance of the material. The recovery of the resistance after removal of LPG is determined by both oxygen re-adsorption from the ambient at the surface and re-oxidation of the oxide [28,29]. The ZnO flakes (sample Z1) showed slower response than the rods, most likely due to complex morphology of the sample. The relatively rapid response and recovery of the resistance of ZnO rods imply that the surface morphology has more significant effect not only on response time but also the recovery rate of the sensor resistance.

3.3.3. *Effect of orientation of rods: H_2O_2 effect*

Fig. 8 shows gas response as a function of operating temperature for ZnO rods (samples Z3, Z31 and Z32) under the exposure of 2600 ppm of LPG. It is observed that, among all the samples, sample Z32 shows the maximum gas response of 38% at 573 K to 2600 ppm of LPG in air, i.e., vertically aligned ZnO rods have shown enhanced gas response than entangled ZnO rods. The enhanced response is attributed to the fact that, vertically aligned morphology of ZnO rods provides not only direct path for efficient electron collection but also provides the variety of channels for surface interactions between chemisorbed oxygen adions and reducing gasses, which

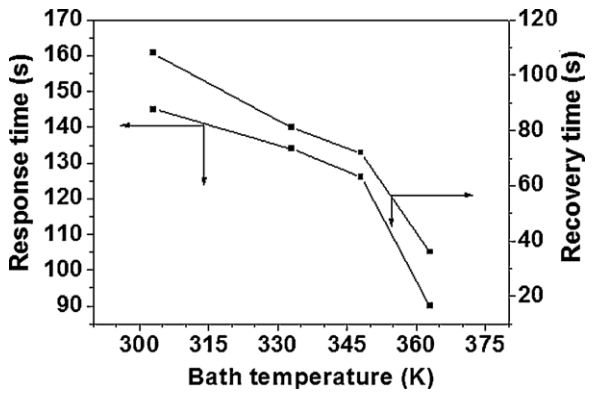

Fig. 7. The response and recovery times for samples Z1–Z4 at operating temperature 673 K upon exposure to 2600 ppm of LPG.

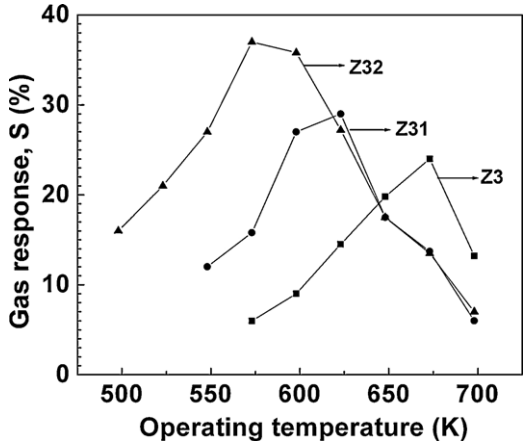

Fig. 8. The gas response as a function of operating temperature for samples Z3, Z31 and Z32 under the exposure of 2600 ppm of LPG.

makes more surface be exposed to the testing gas than in entangled rods. As a result, the sensing properties of vertically aligned ZnO rods were improved [33]. The response of vertically aligned ZnO rods to LPG has shown better than that obtained by Shinde et al. [36] for entangled ZnO rods.

Fig. 9 shows the gas response as a function of operating temperature for vertically aligned ZnO rods (sample Z32), under the exposure of 2600 ppm of LPG in air. From figure it is revealed that sample exhibited maximum response of 38% at 573 K. Further, it can be evident from the figure that the sensor reaches saturation response faster at higher temperature than at the lower temperature. Fig. 10 shows the variation of response and recovery time periods with operating temperatures of sample Z32 under the exposure of 2600 ppm of LPG in air. It can be evidenced from the figure that as operating temperature is increased from 498 to 673 K, the response and recovery time periods were decreased from 525 and 140 s to 360 and 99 s, respectively. The relatively rapid response and recovery at higher operating temperature implied that the operating temperature has more significant effect not only on response time but also the recovery rate of the sample. The vertically aligned ZnO rods show a slower response than the entangled rods, most likely due to the relatively higher degree of LPG adsorption.

3.3.4. Effect of gas concentration on the response of vertically aligned ZnO rods

The response transient curve of sample Z32 operated at 573 K for different concentrations [1300–5200 ppm] of LPG is shown in

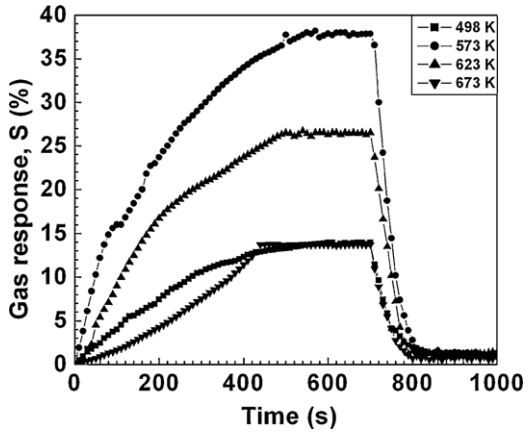

Fig. 9. Response transient curves of sample Z32 obtained at different operating temperatures upon exposure to 2600 ppm of LPG.

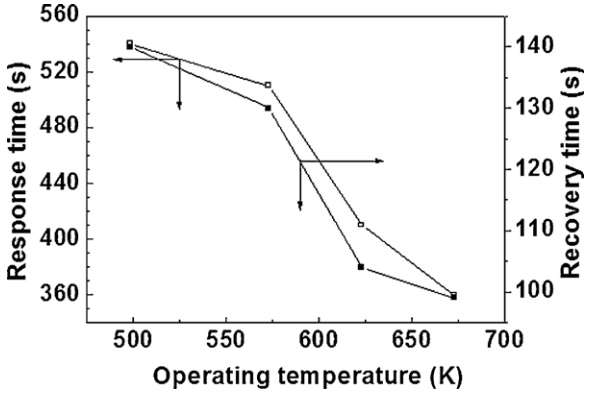

Fig. 10. The variation of response and recovery time of sample Z32 exposed to 2600 ppm of LPG at different operating temperatures.

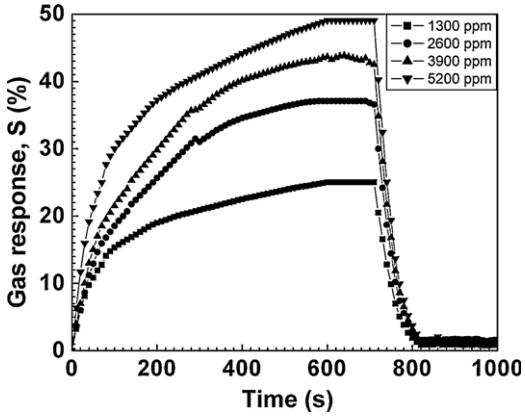

Fig. 11. Response transient curve of sample Z32 obtained at different LPG concentrations operated at 573 K.

Figs. 11 and 12 shows the variation of sensitivities with gas concentration. It is found that the sensitivity of sensor increased as the LPG concentration increased from 1300 to 5200 ppm. Further, it is seen from Fig. 11 that almost the same time (490 s) has been taken to reach the maximum sensitivity for different concentration of gases and the sensitivity dropped rapidly when the gas was removed from testing atmosphere indicating that sensor has good recovery time at higher concentrations of gas. Thus, maximum sensitivity of 49% was obtained at 573 K upon exposure to 5200 ppm of LPG in air, which corresponds to 20% of lower explosion limit (LEL)

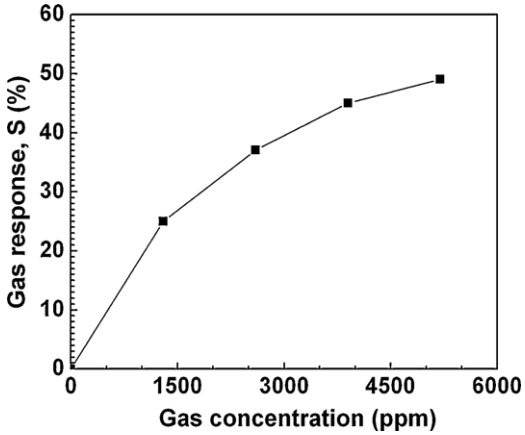

Fig. 12. Variation of response of sample Z32 with LPG concentrations at operating temperature of 573 K.

of LPG. The response of ZnO rods to LPG is certainly better than that obtained by Shinde et al. [37] for ZnO nanobeads where they have obtained the maximum response of 43% under the exposure of 5200 ppm at 673 K and also better than that reported by Sahay and Nath [38].

4. Conclusions

The various ZnO microstructures are synthesized by chemical method. The morphology evolves from flakes to rods with improved crystallinity by increasing bath temperature (303–363 K). Further, vertical alignment of entangled ZnO rods is achieved by adding 2 vol.% H_2O_2 in the bath solution (bath temperature 348 K). ZnO microstructures strongly affect LPG sensing properties. The well-defined ZnO rods show higher gas response than flakes and dense rods for low concentrations of LPG (5–20% of LEL of LPG). Further, enhanced gas response is obtained for vertically aligned ZnO rods. It shows the maximum gas response of 49% to 5200 ppm of LPG at 573 K. This demonstrates that the present route is a facile way to form high-quality ZnO structures for effective LPG sensor.

Acknowledgement

Authors are grateful to the Department of Science and Technology, New Delhi for financial support through the scheme no. SR/S2/CMP-82/2006.This research was partially supported by National Research Foundation of Korea (NRF) Grant funded by the Korean government. One of author KVG is thankfull to Dr. R. S. Kalubarme for having fruitfull discussions.

References

[1] B.A. Buchine, W.L. Hughes, F.L. Degertekin, Z.L. Wang, Nano Lett. 6 (2006) 1155–1159.
[2] D.C. Look, Mater. Sci. Eng. B 80 (2001) 383–388.
[3] Z.L. Wang, J. Phys.: Condens. Matter 16 (2004) 829–858.
[4] A. Amlouk, K. Boubaker, M. Bouhafs, M. Amlouk, J. Alloys Compd. 509 (2011) 3661–3666.
[5] K. Chen, F.Y. Hung, S.J. Chang, S.J. Young, J. Alloys Compd. 479 (2009) 674–677.
[6] J.H. Kim, D.H. Cho, W. Lee, B.M. Moon, W. Bahng, S.C. Kim, N.K. Kim, S.M. Koo, J. Alloys Compd. 489 (2010) 179–182.
[7] K.V. Gurav, V.J. Fulari, U.M. Patil, C.D. Lokhande, O.S. Joo, Appl. Surf. Sci. 256 (2010) 2680–2685.
[8] C. Gu, J. Huang, Y. Wu, M. Zhai, Y. Sun, J. Liu, J. Alloys Compd. 509 (2011) 4499–4504.
[9] K. Matsulbara, P. Fons, K. Iwata, A. Yamada, K. Sakurai, H. Tampo, S. Niki, Thin Solid Films 431 (2007) 369–372.
[10] R. Ten-Zaera, M. Ryan, A. Katty, G. Hodes, S. Bestide, C. Levy-Clement, C.R. Chim. 9 (2006) 717–721.
[11] S.K. Sharma, A.I. Inamdar, H. Im, B.G. Kim, P.S. Patil, J. Alloys Compd. 509 (2011) 2127–2131.
[12] P.K. Baviskar, J.B. Zhang, V. Gupta, S. Chand, B.R. Sankapal, J. Alloys Compd. 510 (2012) 33–37.
[13] C.W. Hsu, T.C. Cheng, C.H. Yang, Y.L. Shen, J.S. Wu, S.W. Wu, J. Alloys Compd. 509 (2011) 1774–1776.
[14] S.L. Wang, X. Jia, P. Jiang, H. Fang, W.H. Tang, J. Alloys. Compd. 502 (2010) 118–122.
[15] J. Li, H. Fan, X. Jia, J. Chen, Z. Cao, X. Chen, J. Alloys Compd. 481 (2009) 735–739.
[16] J.H. Yang, J.H. Zheng, H.J. Zhai, L.L. Yang, Y.J. Zhang, J.H. Lang, M. Gao, J. Alloys Compd. 475 (2009) 741–744.
[17] K.V. Gurav, U.M. Patil, S.M. Pawar, J.H. Kim, C.D. Lokhande, J. Alloys Compd. 509 (2011) 7723–7728.
[18] E. Hosono, S. Fujihara, I. Honma, H. Zhou, Adv. Mater. 17 (2005) 2091–2094.
[19] P. Ma, Y. Wu, Z. Fu, W. Wang, J. Alloys Compd. 509 (2011) 3576–3581.
[20] S.B. Kulkarni, U.M. Patil, R.R. Salunkhe, S.S. Joshi, C.D. Lokhande, J. Alloys Compd. 509 (2011) 3486–3492.
[21] F. Xu, Y. Lu, Y. Xie, Y. Liu, J. Phys. Chem. C 113 (2009) 1052–1059.
[22] Z.N. Urgessa, O.S. Oluwafemi, J.R. Botha, Physics B: Condens Matter. Available online 28 September 2011.
[23] R.C. Pawar, J.S. Shaikh, A.A. Babar, P.M. Dhere, P.S. Patil, Sol. Energy 85 (2011) 1119–1127.
[24] J. Duan, X. Liu, Q. Han, X. Wang, J. Alloys Compd. 509 (2011) 9255–9263.
[25] K. Yuan, X. Yin, J. Li, J. Wu, Y. Wang, F. Huang, J. Alloys Compd. 489 (2010) 694–699.
[26] D.S. Dhawale, C.D. Lokhande, J. Alloys Compd. 509 (2011) 10092–10097.
[27] B. Yuliarto, M. Iqbaal, S. Julia, Nugraha, The Third Nanoscience and Nanotechnology Symposium, 2010.
[28] K.V. Gurav, P.R. Deshmukh, C.D. Lokhande, Sens. Actuators B 151 (2011) 365–369.
[29] C.D. Lokhande, P.M. Gondkar, R.S. Mane, V.R. Shinde, S.H. Han, J. Alloys Compd. 475 (2009) 304–311.
[30] R.B. Birajdar, A. Ghosh, A. Ghule, F. Singh, R. Sharma, Sens. Actuators B 160 (2011) 1050–1055.
[31] R.C. Pawar, J.S. Shaikh, A.V. Mohalkar, S.M. Pawar, J.H. Kim, J.Y. Patil, Sens. Actuators B 151 (2010) 212–218.
[32] S.C. Nawale, S.W. Gosawi, I.S. Mulla, Talanta 75 (2008) 1315–1319.
[33] J.X. Wang, X.W. Sun, Y. Yang, H. Huang, Y.C. Lee, O.K. Tan, L. Vayssieres, Nanotechnology 17 (2006) 4995–5001.
[34] C.C. Lin, S.Y. Chen, S.Y. Cheng, H.Y. Lee, Appl. Phys. Lett. 84 (2004) 5040–5042.
[35] L. Liao, H.B. Lu, J.C. Li, H. He, D.F. Wang, D.J. Fu, C. Liu, J. Phys. Chem. C 111 (2007) 1900–1903.
[36] V.R. Shinde, T.P. Gujar, C.D. Lokhande, R.S. Mane, S.H. Han, Mater. Sci. Eng. B 137 (2007) 119–125.
[37] V.R. Shinde, T.P. Gujar, C.D. Lokhande, Sens. Actuators B 120 (2007) 551–559.
[38] P.P. Sahay, R.K. Nath, Sens. Actuators B 134 (2008) 654–659.